THE JOURNAL OF PHYSICAL CHEMISTRY B
A JOURNAL OF THE AMERICAN CHEMICAL SOCIETY

pubs.acs.org/JPCB

Article

Effect of the Thermal Fluctuations of the Photophysics of GC and CG DNA Steps: A Computational Dynamical Study

Haritha Asha, James A. Green, Luciana Esposito, Lara Martinez-Fernandez, Fabrizio Santoro, and Roberto Improta*

Cite This: https://doi.org/10.1021/acs.jpcb.2c05688

Read Online

ACCESS | Metrics & More | Article Recommendations | Supporting Information

ABSTRACT: Here we refine and assess two computational procedures aimed to include the effect of thermal fluctuations on the electronic spectra and the ultrafast excited state dynamics of multichromophore systems, focusing on DNA duplexes. Our approach is based on a fragment diabatization procedure that, from a given Quantum Mechanical (QM) reference method, can provide the parameters (energy and coupling) of the reference diabatic states on the basis of the isolated fragments, either for a purely electronic excitonic Hamiltonian (FrDEx) or a linear vibronic coupling Hamiltonian (FrD-LVC). After having defined the most cost-effective procedure for DNA duplexes on two smaller fragments, FrDEx is used to simulate the absorption and Electronic Circular Dichroism (ECD) spectra of $(GC)_5$ sequences, including the coupling with the Charge Transfer (CT) states, on a number of structures extracted from classical Molecular Dynamics (MD) simulations. The computed spectra are close to the reference TD-DFT calculations and fully consistent with the experimental ones. We then couple MD simulations and FrD-LVC to simulate the interplay between local excitations and CT transitions, both intrastrand and interstrand, in GC and CG steps when included in a oligoGC or in oligoAT DNA sequence. We predict that for both sequences a substantial part of the photoexcited population on G and C decays, within 50−100 fs, to the corresponding intrastrand CT states. This transfer is more effective for GC steps that, on average, are more closely stacked than CG ones.

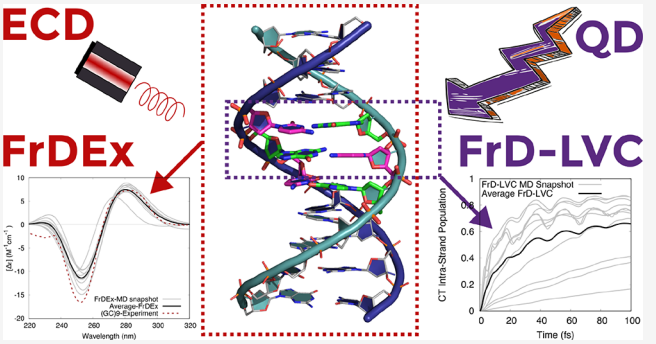

INTRODUCTION

The measurement of an absorption or electronic circular dichroism (ECD) spectrum is one of the first and most basic steps to identify and characterize the static and dynamical behavior of a DNA sequence.[1−5] Indeed, the formation of a DNA duplex is mirrored by typical changes in the UV absorption spectrum relative to the isolated nucleobases, typically manifested as a relatively large hypochromic effect.[1,6,7] At the same time, the different possible duplex conformations, that is, B-DNA, A-DNA, and Z-DNA, are characterized by well-defined ECD signatures.[4,5] Unfortunately, the UV light absorption by DNA has also potentially harmful consequences, since it can trigger a cascade of photophysical and photochemical processes[8−15] that can lead to apoptosis or to the damage of the genetic code and, therefore, to carcinogenesis.[8,11] The study of the interaction between DNA and UV light is thus important from several perspectives, from the (bio)analytical to the (bio)medical one, explaining the huge number of experimental and theoretical studies devoted to characterize the photophysics of oligo- and polynucleotides.[8−15] Independently of the particular aspect of the UV/DNA interaction one is interested in, a proper inclusion of conformational effects is surely important. Despite the overall stability, at room temperature, DNA (and RNA)[16] are fluctuating multichromophore assemblies (MCAs),[17,18] which can exhibit significant deviations from the "average" structure, with consequent different interactions with UV light. For example, small changes in the stacking geometry can significantly alter π-orbital overlap, modifying bright and charge transfer electronic couplings,[19−22] which in turn alter the duplex spectral behavior. Conformational effects are particularly important also to determine the final "outcome" of the photoactivated processes in DNA. Just to make an example, the photodimerization of pyrimidines, one of the two most important photochemical reactions occurring in DNA,[23,24] is strongly modulated by the arrangement of the potentially reacting stacked pyrimidines.[11,15,25−28] Experiments and calculations agree in predicting that, for suitable stacking geometry, this reaction is very effective and ultrafast, with the

Received: August 9, 2022
Revised: November 24, 2022

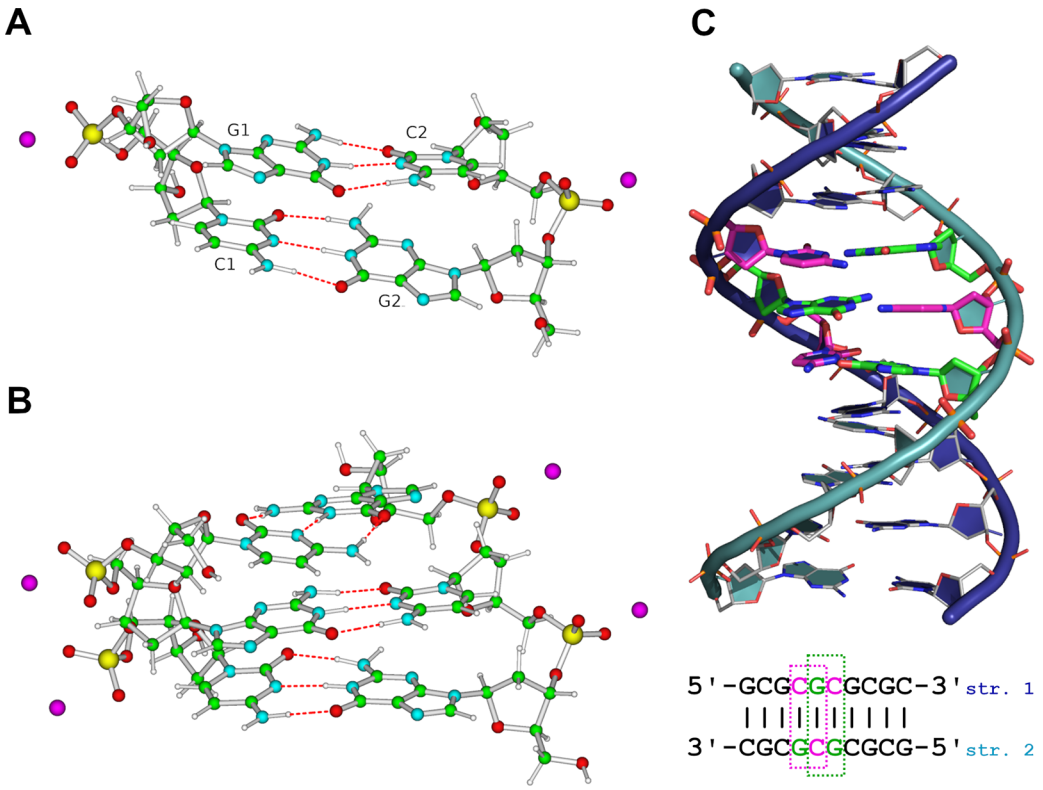

Figure 1. Schematic description of (A) GC and (B) CGC QM models used to tune our FrDEx procedure. (C) $(GC)_5$ system studied by MD simulations. The magenta and green dotted lines in the scheme below encompass, respectively, the CG and the GC steps studied by FrD-LVC QD simulations.

cyclobutane ring formed within 1 ps after the excitation.[25] On the other hand, when the stacked bases are too distant, or their stacking geometry is not the "optimal" one, nonradiative ground state decay is instead the most favored process.[23,26]

In the present study, we thus focus on the inclusion of thermal fluctuations in a computational study of photoexcited DNA using two representative test-cases: (1) the calculation of the absorption and ECD spectra of $(GC)_5$ sequences and (2) the simulation of the photoactivated dynamics of GC and CG steps, in sequences of different flexibility. The ECD spectrum of oligo(GC) duplexes exhibits the "classical" signature of B-DNA conformation,[4,5] and, given the rigidity of GC tracts, is a good test-case to understand how the spectral properties of DNA sequence are affected by small variations of the stacking geometry. Our approach is based on a fragment (Fr) diabatization (D) procedure that we have recently developed to provide the parameters either for a purely electronic excitonic (Ex) Hamiltonian (FrDEx) to simulate spectra of MCAs with a large number of chromophores,[29,30] or a linear vibronic coupling (LVC) Hamiltonian (FrD-LVC)[31,32] for quantum dynamics (QD) simulations.

We have recently profitably applied FrDEx to the study of the spectral properties of guanine-rich sequences folding in quadruple helices (G-Quadruplex, GQ).[29,30] The present study will thus also provide the opportunity to set a suitable strategy for using this approach to compute the ECD signature of B-DNA, a classical test case for many computational approaches (see, for example,[33−38] and references therein). FrD-LVC has instead recently been used to study the competition between intrachromophore internal conversions (e.g., $\pi\pi^* \rightarrow n\pi^*$) and interchromophore excitonic and charge transfer (CT) dynamics in the Watson−Crick GC and AT base pairs.[31,32]

The possible occurrence of CT and Proton Coupled Electron transfer (PCET) processes in oligonucleotides has been the focus of very intense research activity in the last years, as shown, just to cite some of the contributions, by refs 39−50. Moreover, oligonucleotides have been an important playground for many methodological studies dealing with the analysis of CT states and discussing the accuracy of different electronic methods in their treatment.[51−53] For what concerns the double stranded DNA photophysics within a GC or CG step in the present work (see Figures 1 and S3 in the SI), we shall study the interplay between bright, spectroscopic, states and intra- and interstrand CT states. Experiments on $(GC)_9$[48,49,54] and calculations[47−49] predict indeed that in $(GC)_n$ sequences, a significant part of the photoexcited population decays to CT states, which can then trigger PT reactions. We shall compare the behavior of a GC(CG) step included in an alternated oligoGC sequence or in alternated oligoAT sequence (see Scheme 1 below). The stability of DNA duplex significantly depends on stacking interactions,[55−57] the former is indeed expected to be stiffer, considering that three hydrogen bonds per base pair are present, whereas the latter exhibits only two hydrogen bonds per pair.

In both cases, our procedure will be coupled with MD simulations, which will provide a set of snapshots to include thermal fluctuations, in sufficient number for the purposes of the present study, that is, to refine and assess the performances of our approach to investigate DNA duplexes and get additional information on the chemical physical effects modulating their photophysical properties of DNA. We postpone to future studies a detailed analysis of the available experimental results on GC DNA photoactivated dynamics.

https://doi.org/10.1021/acs.jpcb.2c05688
J. Phys. Chem. B XXXX, XXX, XXX−XXX

Scheme 1. DNA Sequences Studied by MD Techniques[a]

(GC)$_5$

```
5'-GCGCGCGCGC-3'  strand 1
   ||||||||||
3'-CGCGCGCGCG-5'  strand 2
```

AGCT

```
5'-GCATATAGCTATATGC-3  strand 1
   ||||||||||||||||
3'-CGTATATCGATATACG-5'strand 2
```

ACGT

```
5'-GCATATACGTATATGC-3  strand 1
   ||||||||||||||||
3'-CGTATATGCATATACG-5'strand 2
```

[a]The bases, whose dynamics have been simulated by FrD-LVC calculations, are depicted in green (G) and in magenta (C).

We show that FrDEx nicely captures the effect of the duplex formation on the absorption and the ECD spectra of B-DNA, and provide spectra very close to the reference QM spectra used for its parametrization, that is, PCM0TD-DFT calculations, with the M05-2X functional.

For what concerns QD simulations, this study demonstrates that FrD-LVC can treat the photoactivated dynamics in a system including several bases, a dozen excited states, and ≥100 vibrational modes. Confirming previous indications,[45,48] we show that the bright excited states localized on G and C are strongly coupled to intrastrand CT states, especially for GC steps. Such CT states are substantially populated on an ultrafast time-scale, independently of the DNA sequence considered. The fairly limited computational cost of FrDEx and FrD-LVC makes the inclusion of thermal fluctuations by MD simulations fully feasible.

METHODOLOGICAL PROCEDURES

Fragment Diabatization. The FrD procedure has been described in detail in previous works[29,31] and is therefore only briefly sketched below. It is an adiabatic-to-diabatic transformation, which utilizes Löwdin orthogonalization

$$|\boldsymbol{d}\rangle = |\boldsymbol{a}^{\mathrm{MCA}}\rangle \boldsymbol{D} = |\boldsymbol{a}^{\mathrm{MCA}}\rangle \boldsymbol{S}^T(\boldsymbol{S}\boldsymbol{S}^T)^{-1/2} \tag{1}$$

to go from adiabatic states computed on a MCA ($|\boldsymbol{a}^{\mathrm{MCA}}\rangle$) to diabatic states $|\boldsymbol{d}\rangle$, which resemble reference states $|\boldsymbol{R}\rangle$ defined on individual chromophores. These reference states are either adiabatic states of individual chromophores for local excitations (LEs), or one electron transitions between an occupied orbital on one fragment and a virtual orbital on another for CT states. They are used to compute the overlap matrix $\boldsymbol{S}$, defined as $\boldsymbol{S} = \langle \boldsymbol{R}|\boldsymbol{a}^{\mathrm{MCA}}\rangle$ with elements $S_{ir} = \langle R_i|a_r^{\mathrm{MCA}}\rangle$, from which transformation matrix $\boldsymbol{D}$ is obtained. The similarity of the diabatic states to the reference states can be monitored by computing the overlap $\langle \boldsymbol{R}|\boldsymbol{d}\rangle$, that is, $\boldsymbol{S}\boldsymbol{S}^T(\boldsymbol{S}\boldsymbol{S}^T)^{-1/2}$, and ensuring it is close to the identity matrix.

This transformation matrix can then be applied to the diagonal matrix of MCA adiabatic energies $H[\boldsymbol{a}^{\mathrm{MCA}}]$ to yield a matrix of diabatic energies and couplings

$$H[\boldsymbol{d}] = \boldsymbol{D}^T H[\boldsymbol{a}^{\mathrm{MCA}}]\boldsymbol{D} \tag{2}$$

which are then used to paramaterize the FrDEx and FrD-LVC models, described below.

FrDEx. For FrDEx, an excitonic state k for a system of N_{mol} chromophores is written as

$$|\Psi^k\rangle = \sum_m^{N_{\mathrm{mol}}} \sum_\alpha^{N_{\mathrm{loc}}} C_m^{\alpha,k}|\mathrm{L}_\alpha^m\rangle + \sum_m^{N_{\mathrm{mol}}} \sum_{n\neq m}^{N_{\mathrm{mol}}} \sum_\gamma^{N_{\mathrm{CT}}} C_{mn}^{\gamma,k}|\mathrm{CT}_\gamma^{m\to n}\rangle \tag{3}$$

where, for each chromophore m, the index α labels the N_{loc} possible LEs (L_α^m) with a corresponding coefficient $C_m^{\alpha,k}$. The index γ identifies the N_{CT} different types of CT states ($\mathrm{CT}_\gamma^{m\to n}$) where an electron is transferred from monomer m to monomer n, with corresponding coefficient $C_{mn}^{\gamma,k}$.

The FrDEx Hamiltonian on the basis of these LE and CT states is then written as

$$\begin{aligned}
H_{\mathrm{FrDEx}} &= H_{\mathrm{intra}} + H_{\mathrm{inter}}\\
H_{\mathrm{intra}} &= \sum_m^{N_{\mathrm{mol}}} \left\{ \sum_\alpha^{N_{\mathrm{loc}}} \left[E_{\mathrm{L}_\alpha^m}|\mathrm{L}_\alpha^m\rangle\langle \mathrm{L}_\alpha^m| \right] \right\} + \sum_{\beta\neq\alpha}^{N_{\mathrm{loc}}} E_{\mathrm{L}_\alpha^m,\mathrm{L}_\beta^m}(|\mathrm{L}_\alpha^m\rangle\langle \mathrm{L}_\beta^m| + \mathrm{h.\,c.})\\
H_{\mathrm{inter}} &= \sum_m^{N_{\mathrm{mol}}} \sum_{n\neq m}^{N_{\mathrm{mol}}} \left\{ \sum_{\alpha,\beta}^{N_{\mathrm{loc}}} E_{\mathrm{L}_\alpha^m,\mathrm{L}_\beta^n}(|\mathrm{L}_\alpha^m\rangle\langle \mathrm{L}_\beta^n| + \mathrm{h.\,c.}) \right.\\
&\quad + \sum_\gamma^{N_{\mathrm{CT}}} [E_{\mathrm{CT}_\gamma^{m\to n}}|\mathrm{CT}_\gamma^{m\to n}\rangle\langle \mathrm{CT}_\gamma^{m\to n}|\\
&\quad + \sum_{\delta\neq\gamma}^{N_{\mathrm{CT}}} E_{\mathrm{CT}_\gamma^{m\to n},\mathrm{CT}_\delta^{m\to n}}(|\mathrm{CT}_\gamma^{m\to n}\rangle\langle \mathrm{CT}_\delta^{m\to n}| + \mathrm{h.\,c.})\\
&\quad + \sum_\delta^{N_{\mathrm{CT}}} E_{\mathrm{CT}_\gamma^{m\to n},\mathrm{CT}_\delta^{n\to m}}(|\mathrm{CT}_\gamma^{m\to n}\rangle\langle \mathrm{CT}_\delta^{n\to m}| + \mathrm{h.\,c.})\\
&\quad + \sum_\alpha^{N_{\mathrm{loc}}} (E_{\mathrm{L}_\alpha^m,\mathrm{CT}_\gamma^{m\to n}}(|\mathrm{L}_\alpha^m\rangle\langle \mathrm{CT}_\gamma^{m\to n}| + \mathrm{h.\,c.})\\
&\quad \left. + E_{\mathrm{L}_\alpha^m,\mathrm{CT}_\gamma^{n\to m}}(|\mathrm{L}_\alpha^m\rangle\langle \mathrm{CT}_\gamma^{n\to m}| + \mathrm{h.\,c.}))] \right\}
\end{aligned} \tag{4}$$

where H_{FrDEx} is split into an intramolecular part H_{intra} and an intermolecular part H_{inter}, and h.c. stands for Hermitian conjugate.

The intramolecular part contains only the LE energies, $E_{\mathrm{L}_\alpha^m}$, and the couplings of different LEs on the same chromophore, $E_{\mathrm{L}_\alpha^m,\mathrm{L}_\beta^m}$. The intermolecular part contains all other terms involving more than one chromophore (i.e., all terms involving CT states and the excitonic coupling $E_{\mathrm{L}_\alpha^m,\mathrm{L}_\beta^n}$). These parameters are all obtained through application of the FrD procedure, and as described previously,[29,30] splitting the Hamiltonian into H_{intra} and H_{inter} portions allows them to be parametrized on the basis of adiabatic states of different sized subsets of the entire N_{mol} MCA to best balance accuracy and computational efficiency. In these prior works, we have referred to this subset of the entire MCA as a "supra-molecular complex" (SC), utilized dimer calculations for H_{inter}, and demonstrated that π-stacked strands are the most effective method to parametrize H_{intra} and account for changes in LE character and mixing due to surrounding monomers.

FrD-LVC. The LVC Hamiltonian for a coupled set of diabatic electronic states $|\boldsymbol{d}\rangle = (|d_1\rangle, |d_2\rangle, ..., |d_j\rangle)$ may be written as[58]

https://doi.org/10.1021/acs.jpcb.2c05688
J. Phys. Chem. B XXXX, XXX, XXX−XXX

Scheme 2. Schematic Description of Some Possible Choices for the SC Used in the FrDEx Model[a]

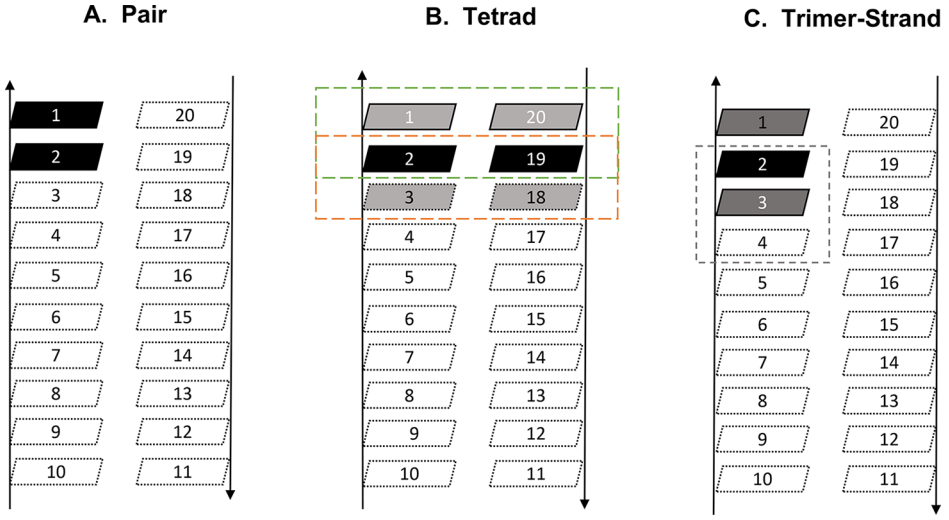

[a](a) Dimer; (b) Tetrad - green and red dashed lines identify the two "tetrads" used to compute H_{intra} terms for bases 2 and 19; (c) Strand. The colored bases identify the SC used to compute H_{intra} terms for bases 1 and 2. The dashed grey rectangle shows the system used to compute H_{intra} for base 3.

$$H = \sum_i (K + V_{ii}^{d}(\mathbf{Q})|d_i\rangle\langle d_i|) + \sum_{i,j>i} V_{ij}^{d}(\mathbf{Q}) (|d_i\rangle\langle d_j| + |d_j\rangle\langle d_i|) \quad (5)$$

where $\{Q_1, Q_2, ..., Q_\nu\}$ are the dimensionless normal mode coordinates, defined in the ground electronic state S_0, with conjugate momenta $\boldsymbol{P}$. The kinetic K and potential V terms of the Hamiltonian are defined as

$$K = \frac{1}{2}\boldsymbol{P}^T\boldsymbol{\Omega}\boldsymbol{P} \quad (6)$$

$$V_{ii}^{d}(\mathbf{Q}) = E_{ii}^{d}(\mathbf{Q}_0) + \boldsymbol{\lambda}_{ii}^T\mathbf{Q} + \frac{1}{2}\mathbf{Q}^T\boldsymbol{\Omega}\mathbf{Q} \quad (7)$$

$$V_{ij}^{d}(\mathbf{Q}) = E_{ij}^{d}(\mathbf{Q}_0) + \boldsymbol{\lambda}_{ij}^T\mathbf{Q} \quad (8)$$

with $\boldsymbol{\Omega}$ being the diagonal matrix of normal-mode frequencies ω_μ, $\boldsymbol{\lambda}_{ij}$ is the vector of linear coupling constants between states i and j, $E_{ii}^{d}(\mathbf{Q}_0)$ is the diabatic energy of state i at the reference geometry ($\mathbf{Q}_0$, typically a ground state equilibrium geometry, see Computational Details for further information), and $E_{ij}^{d}(\mathbf{Q}_0)$ is an electronic coupling constant between diabatic states i and j at the reference geometry. The constant energies and couplings E_{ij} are obtained by applying the FrD scheme at the reference geometry, and they are exactly equivalent to those in the FrDEx model, reported in eq 4. The gradient coupling terms $\boldsymbol{\lambda}_{ij}$ are obtained by applying the FrD scheme at small displacements along the normal mode coordinates and then performing a numerical differentiation.[31]

COMPUTATIONAL DETAILS

MD Simulations. We have performed 2 μs long MD simulations for three different sequences of DNA duplexes containing GC and/or CG steps. In particular, we studied the 10mer sequence $(GC)_5$ and the 16mer sequences GCAT-ATAGCTATATGC and GCATATACGTATATGC, where either a GC or a CG step is embedded in a AT repetitive sequence (GC bases at the termini were added to avoid fraying ends; herein we denote these two duplexes as AGCT and ACGT, respectively). All the starting B-DNA models were built by the web 3DNA 2.0 server.[59] The duplex structure was solvated in a truncated octahedral water box with the distance between solute and box border being at least 10 Å. The water SPC/E model was used.[60] The system was first neutralized by Na^+ ions and then 0.15 M NaCl was added; the ions parameters were derived by Joung and Cheatham.[61] The simulations were carried out with the OL15 force field.[62] Before the production run, a standard equilibration protocol was employed. The system was minimized by 500 steps of steepest descent minimization followed by 500 steps of conjugate gradient minimization with 25 kcal mol^{-1} Å^{-2} position restraints on DNA atoms. We then imposed position restraints of 25 kcal mol^{-1} Å^{-2} on the DNA molecule and heated the system from 100 to 300 K over 100 ps. During the heating process, the volume was kept constant. The system was then minimized with 5 kcal mol^{-1} Å^{-2} restraints on the DNA fragment by 500 steps of steepest descent method followed by 500 steps of the conjugate gradient optimization approach. The whole system was then equilibrated for 50 ps at constant pressure and temperature of 1 bar and 300 K, respectively. The series of consecutive minimization and equilibration steps, as described above, were performed by applying decreasing restraints on the atomic position of the DNA fragment of 4, 3, 2, 1, and 0.5 kcal mol^{-1} Å^{-2}. The final equilibration step was followed by 50 ps of unrestrained molecular dynamics simulation. Temperature and pressure coupling constants were set to 0.2 ps during the equilibration and to 5 ps during the final free molecular dynamics run, as well as during the production run. A 2 μs production run was started afterward and coordinates were saved every 5 ps. We used the Berendsen weak-coupling thermostat and barostat.[63] Electrostatic interactions were treated using the Particle Mesh Ewald method (PME). The nonbonded cutoff was set to 9 Å. Simulations were carried out using the CUDA accelerated pmemd module of AMBER 18 MD package.[64] The structures of the trajectories were processed and analyzed by cpptraj amber program, as well as by x3dna (v2.3.4)/dssr (v1.9.9) programs.[65,66]

https://doi.org/10.1021/acs.jpcb.2c05688
J. Phys. Chem. B XXXX, XXX, XXX−XXX

We have analyzed specific structural properties for the structures of the whole trajectories as well as for a subset of structures extracted from each trajectory. To avoid bias from the selection criterion, we simply considered an adequate number of structures that can be handled by our subsequent QD calculations and picked them from the trajectory by extracting frames every 200 ns interval (a total of 11 structures were considered: 10 plus 1 structure at the start of the production run, t = 0 ns).

Reference Electronic Structure. We utilize Time-Dependent (TD)-DFT, as implemented in the *Gaussian 16* package,[67] to compute adiabatic states that are used in the FrD procedure to parametrize the FrDEx and FrD-LVC models, as well as to provide reference absorption and ECD spectra. We have selected the M05-2X functional,[68] which can reliably describe CT transitions in stacked systems, as shown also by previous studies on oligonucleotides,[15] and the 6-31G(d) basis set. Solvent effect of water has been included via the Polarizable Continuum model (PCM).[69] For comparison, we also compute absorption and ECD spectra with an excitonic model in which only LEs are included, and the excitonic coupling between them is computed via the Coulombic interaction between transition densities. We denote this approach as a Frenkel Hamiltonian with Coulombic couplings (FHC) and is computed with the "EET" option in *Gaussian 16*.[70]

FrDEx. The reference states used to define the diabatic states included in the FrDEx Hamiltonian (eq 4) are the first two bright excited ($\pi\pi^*$) states of each base and 4 CT states for each base pair (2 from G → C and 2 from C → G). CT transitions are defined as the one electron transfer from HOMO of one base to LUMO/LUMO+1 of the other base. For the parametrization of H_{inter}, the reference states are projected onto 40 adiabatic states of all nearest-neighbor dimers, which include stacked pairs, hydrogen bonded pairs and diagonally opposite pairs. For the parametrization of H_{intra}, we tested projection of the reference LE states onto 30 adiabatic states of either a stacked trimer or a hydrogen-bonded and stacked tetrad (see Scheme 2). For both H_{inter} and H_{intra}, we ensured complete projection of the reference states onto the adiabatic states by monitoring the eigenvalues of $\boldsymbol{S}\boldsymbol{S}^T$ and verifying they were close to 1. Paramaterization of H_{inter} required more adiabatic states to be projected onto than H_{intra}, as some of the CT states lay relatively high in energy. In both cases we included the electrostatic effects of the surrounding bases on both the reference and adiabatic states with restrained electrostatic potential (RESP) charges, computed for each base in its ground state. The diabatization was performed with our code *Overdia*, which is freely available.[71]

For most of the FrDEx calculations, the sugar phosphate backbone of the DNA is stripped and the guanine/cytosine nucleotide replaced by optimized 9-methyl guanine/1-methyl cytosine at M05-2X/6-31G(d)/PCM in the C_s symmetry by minimizing the RMSD between them. In the following we shall refer to this approach as the "standard" one. However, the effect of this geometry substitution on the spectra is first evaluated in the Results section.

In order to test the accuracy of FrDEx spectra, we have also used two smaller model compounds (see Figure 1), namely, a GC duplex with two stacked base pairs, and CGC with 3 stacked base-pairs, arranged in B-DNA conformation. These models have been fully optimized, including the phosphodeoxyribose backbone, and their absorption and ECD spectra have been computed at the PCM/TD-M05-2X/6-31G(d) level.[72]

Simulation of the Spectra. The accuracy of the FrDEx spectra also depends on the accuracy of the reference QM method. TD-DFT has well-known limitations, inter alia, in the treatment of excited states with significant CT character.[51,73−75] Many of these drawbacks can be avoided by choosing a suitable functional,[51,68] sometimes at expense of the accuracy in the determination of the excitation energies of the bright states. Actually, the PCM/M05-2X/6-31G(d) computed transition energies of the isolated G and C bases are blue-shifted with respect to the maxima of the experimental absorption bands in solution. This discrepancy is partially due to the lack of vibrational and thermal effects, which significantly red-shifts, by 0.1−0.2 eV, the computed absorption maxima with respect to the vertical transition energies.[76] However, most of the error arises from other limitations of our computational approach (density functional, basis set, lack of explicit solute−solvent interactions), whose selection is dictated by the necessity of having QM reference data for very large size systems, with a reasonable compromise between accuracy and computational cost. As a consequence, in order to enable a more direct comparison with the experimental spectra the TD-DFT, FHC, and FrDEx spectra are shifted by −0.75 eV. Actually, this value allows almost to superimpose the PCM/TD-M05-2X computed vertical transitions of dC and dG in water with the maxima of the corresponding experimental spectra,[77,78] suggesting that the main cause of the discrepancy between experimental and computed spectra are the inaccuracies in the description of the isolated nucleobases. This conclusion is supported by test FrDEx calculations, where the energy of all the LE has been shifted by 0.75 eV, before computing the spectra. As shown in Figure S16 in the SI, the resulting spectrum, unshifted, is indeed very similar to the shifted one. Moreover, the FrDEx spectrum computed using ωB97XD results has a very similar shape to that based on M05-2X, but for red-shift of 0.1−0.15 eV, which corresponds to the red-shift found in the computed transition energies of G and C (Figure S16). All stick transitions are also phenomenologically broadened with a Gaussian with standard deviation of 0.21 eV, that is, the same used in our previous studied on GQ,[29,30] and calculated using a modified version of the EXAT code.[79] However, in the SI (see Figure S17) we report the spectra computed by using different values of the shift and of the width of the broadening Gaussian, showing that our conclusions do not qualitatively depend on the choice of these parameters.

FrD-LVC. FrD-LVC models were constructed for GC and CG tetrads, each containing 12 diabatic states, namely, the lowest two $\pi\pi^*$ states on each G (labeled as G1/G2(L_a), G1/G2(L_b), and C base (labeled as C1/C2($\pi\pi^*1$) and C1/C2($\pi\pi^*2$)), together with the inter- (labeled as G1 → C2(CT), G2 → C1(CT)) and intrastrand (labeled as G1 → C1(CT), G2 → C2(CT)) CT states from the HOMO of G to LUMO of C, that is, the lowest energy CT states. We considered molecular models of G and C as 9-methylguanine and 1-methylcytosine in C_s symmetry, which can reliably model the main features of the excited electronic states of the corresponding nucleosides/nucleotides.[77,78] To reduce the computational burden of the QD simulations, we included only the in-plane vibrational modes of each base, for a total of 124 normal modes. This 124 mode LVC model was fully paramaterized with computations at the QM minimum

https://doi.org/10.1021/acs.jpcb.2c05688
J. Phys. Chem. B XXXX, XXX, XXX−XXX

structures of GC and CG tetrads, and then the zero order terms (i.e., diabatic excited state energies and excitonic/CT-like couplings, E_{ij}) of the LVC model were updated using central GC and CG tetrad structures extracted from the MD simulations of $(GC)_5$ and GC/CG in an AT tract, as shown in Scheme 1. These zero-order terms are those expected to change most significantly from snapshot to snapshot and, hence, will rule the dynamics. The structures extracted from the MD simulation were stripped of the sugar phosphate backbone of DNA and the guanine/cytosine nucleotide replaced by optimized 9-methyl guanine/1-methyl cytosine (at M05-2X/6-31G(d)/PCM level) by minimizing the RMSD between them, the same procedure as the "standard" approach in FrDEx, discussed above.

The parametrization of the LVC model was conducted with the *Overdia* code. QD propagations using the FrD-LVC models were performed using the ML-MCTDH method[80,81] implemented within the Quantics package.[82,83] We followed the numerical procedures used previously in setting up the calculations.[31]

RESULTS

Absorption and ECD Spectra of $(GC)_5$. *Setting up the FrDEx Procedure.* As a first step, before tackling the computation of the spectra of $(GC)_5$, we tune our procedure on two smaller systems, GC and CGC (see Figure 1). For these systems, fully QM reference results are available,[72] that is, computed at the PCM/TD-M05-2X level, including the phosphodeoxyribose backbone both in the geometry optimization and in the calculation of the spectra, thus, providing useful information on the possible source of errors of our treatment. In Figure 2, we compare the ECD spectra computed for GC (both at the QM and FrDEx level) with two different choices for the nucleobases geometry, that is, either the geometries optimized within the duplex (GC-min) or a "standard" one using the minima of the isolated monomers. The standard approach leads to the slight blue-shift of the spectra and to the overestimation of the intensity of the positive lobe at ∼290 nm. Both FrDEx plots are in good agreement with the reference QM, but for a small blue-shift of the positive lobe at ∼290 nm, whose intensity is also further overestimated. Finally, the inclusion of the phosphodeoxyribose backbone has a small effect on the position of the spectrum, but leads to an increase of the intensity of the negative minimum at ∼260 nm and a decrease of the intensity of the positive lobes. The positive lobe at ∼220 nm almost disappears when backbone is included. On the other hand, it is not possible to discuss the prediction of our calculations in the high-energy region of the spectrum, since it could be affected by higher excited states not included in our treatment.

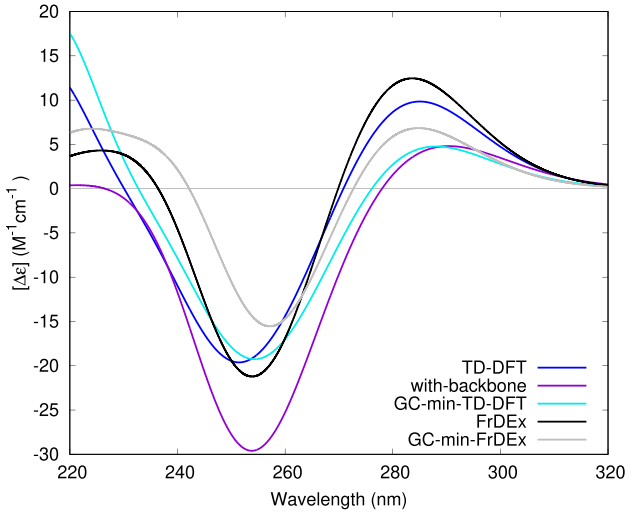

Figure 2. ECD spectra of GC tetrad computed within the QM minimum at the TD-DFT (cyan) or FrDEx (gray) levels. The TD-DFT spectra computed including the backbone are reported in purple. The spectra computed by using the geometry minima of the isolated bases are reported in blue (TD-DFT) or in black (FrDEx). All spectra are shifted by −0.75 eV.

In Figure 3, for CGC we compare the QM reference with the FrDEx spectra computed with two different choices for the SC used to compute H_{intra}. In one case we used the two strands (trimer strand approach, see Scheme 2), and in the other we used the two GC "tetramers"[38] (tetrad approach, averaging the values found for the central bases). The former procedure includes the effect, at the QM level, of the stacked bases within a single calculation. The latter includes, at the QM level, the possible effect on H_{intra} of the complementary strand, which in the "strand" approach is considered only at the classical level (by using atomic charges.)

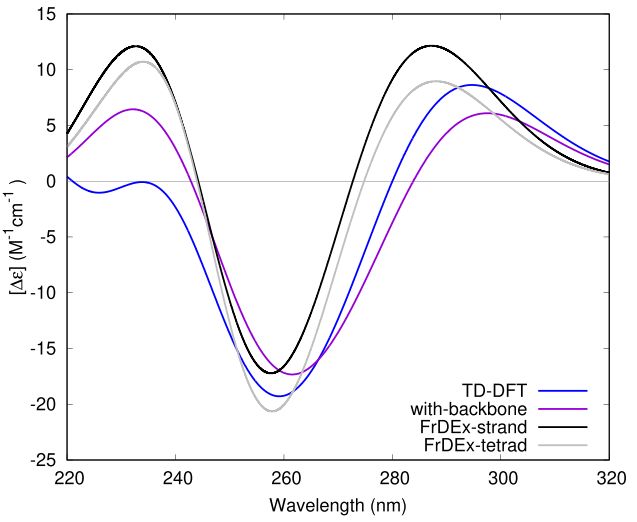

Figure 3. ECD spectra of CGC calculated using FrDEx with H_{intra} parametrized from tetrad (gray, see Scheme 2B) and trimer strand (black, see Scheme 2C) and H_{inter} parametrized from pairs compared with TD-DFT spectra with (purple) or without backbone (blue). All spectra are shifted by −0.75 eV.

On balance, both strategies allows a fairly good reproduction of the QM reference, but for the blue-shift of the positive feature at ∼290 nm we have already discussed above. Tetrad spectra better reproduce the relative intensity of the two main feature of the spectrum. On the other hand, test calculations on $(GC)_5$ (see Figure S7 in the SI), provide the opposite indication. Moreover, the tetrad procedure, which requires two calculations on a tetramer, is slightly computationally more expensive than the strand one (two calculations on a trimer). As a consequence, in the following, if not otherwise specified, our analysis will be based on the "trimer strand" procedure (see Scheme 2), that is, estimating the H_{intra} elements of each base including in the SC the two stacked partners in the same strand (rolling trimer strand approach).

https://doi.org/10.1021/acs.jpcb.2c05688
J. Phys. Chem. B XXXX, XXX, XXX−XXX

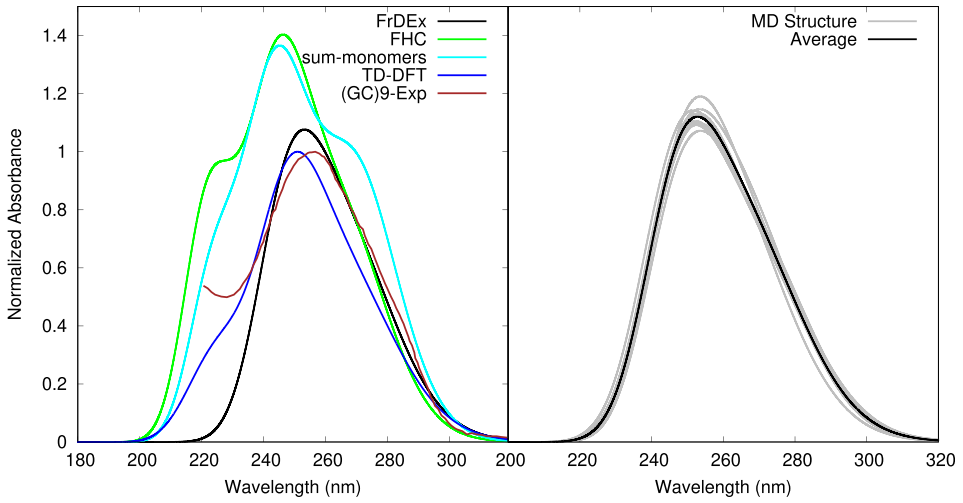

Figure 4. (left) Computed absorption spectra of GC5 at time 0 ns of MD trajectory with FHC and FrDEx compared with sum of monomers. In brown we show the experimental absorption spectrum of $(GC)_9$, normalized with respect to the TD-DFT one, adapted with permission from ref 48. Copyright 2015 American Chemical Society. (right) Calculated absorption spectra of all MD structures (gray) and their average (black) studied using the FrDEx method. All spectra are shifted by −0.75 eV.

As shown in the SI (see Figure S8), including the effect of the other bases on a given SC at a classical level (by means of point RESP charges) has a small effect on the computed GC signal. However, interestingly, the intensity of the negative peak at ∼250 nm increases, thus improving the agreement with the experimental spectra, with a minuscule computational cost.

Absorption Spectra. In Figure 4 (left panel) we show the absorption spectrum computed for one of the $(GC)_5$ structures extracted from MD simulations (that at time = 0), by using TD-DFT, FrDEx, and a standard Frenkel excitonic Hamiltonian (FHC, see Computational Details). For comparison, we also show the experimental spectrum of $(GC)_9$ and that built, simply, as the sum of the computed spectra of 10 G and 10 C monomers. The FrDEx spectrum is in good agreement with the TD-DFT ones, but for a weak red shift of the computed maximum and a small overestimation (less than 10%) of the intensity of the band maximum. Not surprisingly, the agreement with the reference QM results is worse on the blue wing of the absorption band (below 240 nm), simply due to the absence of the higher-lying bright excited states in the FrDEx calculation. FrDEx predicts that the absorption spectrum of $(GC)_5$ is significantly less intense than the sum of monomer spectra, thus reproducing the well-known hypochromic effect associated with the formation of DNA duplex.[1,6,7] On the contrary, the maximum of the FHC spectrum is blue-shifted with respect to that of TD-DFT one, and more significantly, it is much more intense. In fact, its maximum is even slightly more intense that the sum of the monomer spectra, with an almost coincident total absorptivity. The different methods also provide different band shapes. However, we shall not analyze this point in detail, since the computed band shape depends also on the value used for the broadening Gaussian (somewhat arbitrary) and on the number of structures used in the conformational averaging procedure.

In the right panel of Figure 4, we show as gray lines the absorption spectra computed by FrDEx for each of the structures extracted from the MD, and in black is their average. It is clear that, even in a stiff system as $(GC)_5$, thermal effects modulate slightly the measured absorption spectrum, with the intensity of the individual band maxima differing by up to 10%. In any case, the average intensity in the maximum is ∼40% lower than the sum of the monomer spectrum (shown in 4, left panel). This value is fully consistent with that typically associated with the formation of DNA duplexes.[1] On the other hand, as shown in the SI (Figure S9), FHC does not capture this important experimental effect, even when the average over the different structures is considered, and so standard excitonic models are not suitable to reproduce the hypochromic effect in DNA.

ECD Spectra. In Figure 5, we compare the experimental ECD spectrum of $(GC)_9$ with the average ECD spectra computed by using FrDEx or FHC Hamiltonians on the

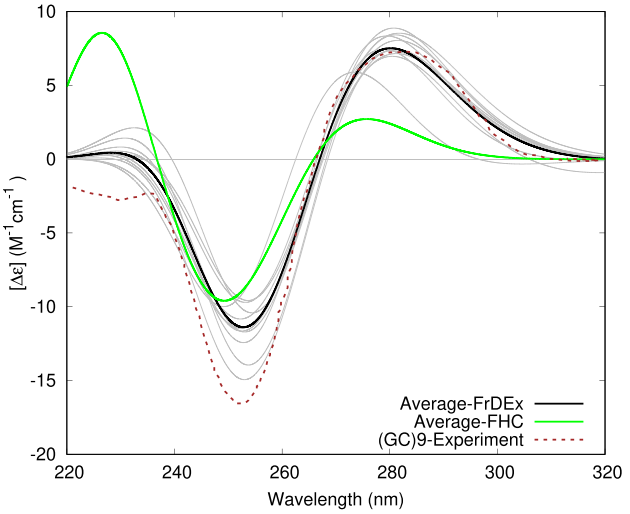

Figure 5. Computed ECD spectra of GC_5 for different structures extracted from MD trajectory (in gray), their average is plotted in black. All FrDEx calculations use rolling trimers as the SC to calculate H_{intra} and pair as the SC to calculate H_{inter}. All spectra are shifted by −0.75 eV. For comparison, in dashed brown we show the experimental ECD spectrum of $(GC)_9$, adapted with permission from ref 48. Copyright 2015 American Chemical Society. In order to get an easier comparison with calculations, the intensity of the experimental spectrum is multiplied by a factor of 2.2.

https://doi.org/10.1021/acs.jpcb.2c05688
J. Phys. Chem. B XXXX, XXX, XXX−XXX

different structures extracted from MD simulations. FrDEx reproduces well the shape and position of the experimental spectra. Considering that the shift of the spectrum has been tuned on the absorption spectra of the separated monomers (no additional adjustment has thus been performed to match oligonucleotide ECD, see also Figure S16), the FrDEx method fairly well captures the effect that the formation of the duplex has on the optical properties of the bases. Our calculations overestimate the intensity of the positive peak at ∼280 nm (the intensity of the experimental spectrum has been multiplied by 2.2), but the relative intensity of the positive lobe at ∼290 nm and the negative one at ∼250 nm is quite satisfactorily reproduced, though the latter one is too weak. However, the relative intensity of the negative peak is also sensitive to the behavior of the high energy region of the spectrum (in the region 200−240 nm), whose treatment would require a much larger number of excited states. On the other hand, the FHC spectrum, though capturing the typical ECD signature of B-DNA, is slightly blue-shifted with respect to FrDEx, and underestimates quite significantly the intensity of the positive ∼290 nm lobe. This feature could be related to the absence of CT states in this method. Indeed, as shown in Figure S11 of the SI, many low-energy excitonic states have a noticeable contribution from CT diabatic states. Though all the spectra have a similar shape, the position and the relative intensity of the lobes quite significantly vary from one structure to another, indicating that our approach could also provide insights into the effect modulating the ECD spectra. A more detailed analysis is however outside the scope of the present paper.

Interplay between Bright and CT States in GC and CG Steps. *Some Insights on the Conformational Dynamics of GC and CG Steps.* We have analyzed the conformational behavior of GC and CG steps in different contexts, that is, central tetrads in either GC or AT repetitive sequences as detailed in Scheme 1. In particular, we have focused our attention on the stacking geometry of the two steps, by analyzing the distance between the purine and pyrimidine rings along the two strands and their overlap. Independently of the duplex considered, our simulations indicate that GC steps are more strongly stacked than CG steps. Indeed in the former step, the two bases are closer (3.7−3.8 Å vs ∼4.4 Å) and their overlap is 4−5× larger (see Table 1). CG steps are slightly more closely stacked when embedded in alternated GC than in AT. Indeed, the interbase stacking distance is slightly shorter, the overlap area larger in this former duplex (see Figure S5 in the SI) On the contrary, for a GC step embedded in AT sequence, the distribution of the distances is narrower and with the maximum shifted at lower values than in $(GC)_5$ sequence. Also the base G-C rings show higher overlap areas in AT repetitive sequences compared to GC repetitive sequences. Hence, the GC step is more stacked in the tetrad AGCT than in the CGCG one The analysis of the root mean squared fluctuations (RMSF; see Figure S6 in the SI) also indicate that GC step is stiffer when embodied in the AT than in the $(GC)_5$ sequence.

Similar stacking geometry trends for CG and GC steps in different sequence contexts are observed in selected PDB experimental structures (Table S14 in the SI), thus confirming the validity of our analysis.

FrD-LVC QD Simulations. In Figures 6 and 7 we report the average results (over the 11 structures considered) of the QD simulations for GC and CG steps following the excitation to one of the three lowest energy bright diabatic states on each strand when included in GC or AT tracts. Confirming the preliminary indications obtained in a parallel characterization of the main singlet deactivation paths in GC sequences,[72] a quite effective and fast population of the intrastrand CT states

Table 1. Stacking Parameters[a]

	distance (Å)		overlap area (Å^2)	
step	mean	StDev	mean	StDev
CG step $(GC)_5$				
C1G1	4.37	0.46	0.57	0.97
C2G2	4.36	0.46	0.60	1.00
ACGT				
C1G1	4.41	0.40	0.46	0.88
C2G2	4.44	0.39	0.38	0.79
GC step $(GC)_5$				
G1C1	3.81	0.30	2.00	1.32
G2C2	3.80	0.29	2.06	1.31
AGCT				
G1C1	3.74	0.21	2.61	1.04
G2C2	3.73	0.21	2.61	1.04

[a]Distance between the centers of mass of the base ring heavy atoms (no exocyclic atoms) belonging to adjacent C and G bases along strands 1 and 2. Overlap area of base ring atoms of adjacent bases along each strand. The overlap area has been calculated by considering the strands separately, that is, treating the whole structure as a continuous single helix.

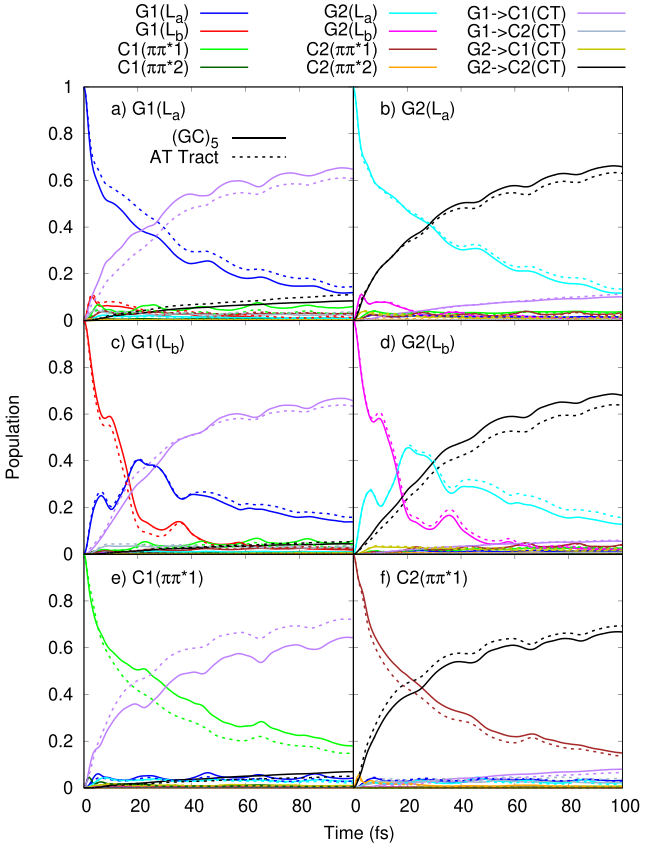

Figure 6. GC tetrad population dynamics following initial excitation to (a) G1(L_a), (b) G2(L_a), (c) G1(L_b), (d) G2(L_b), (e) C1($\pi\pi^*1$), and (f) C2($\pi\pi^*2$). Averaged over snapshots from the $(GC)_5$ (solid lines) and GC in AT tract (dashed) MD simulations.

https://doi.org/10.1021/acs.jpcb.2c05688
J. Phys. Chem. B XXXX, XXX, XXX−XXX

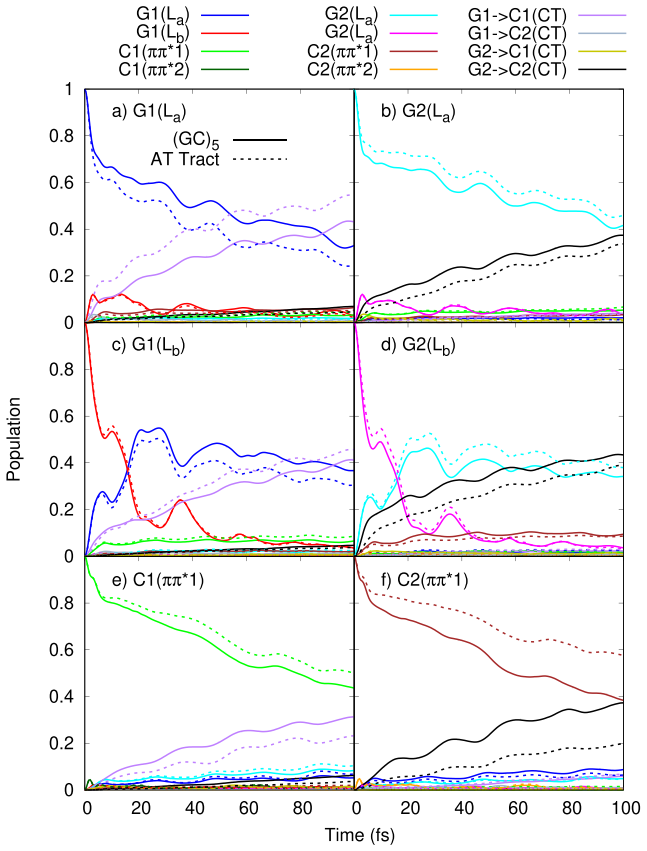

Figure 7. CG tetrad population dynamics following initial excitation to (a) G1(L_a), (b) G2(L_a), (c) G1(L_b), (d) G2(L_b), (e) C1($\pi\pi^*1$), and (f) C2($\pi\pi^*2$). Averaged over snapshots from the $(GC)_5$ (solid lines) and CG in AT tract (dashed) MD simulations.

(G1 → C1-CT and G2 → C2-CT) is predicted, both for GC and CG steps. In the following we shall label the two strands of the duplex as 1 or 2 as they are shown in Figure 1.

In detail, for the GC steps, on average, after 100 fs more than 60% of the excited state population is on G1 → C1-CT when the spectroscopic states are on G1 or C1, or on G2 → C2-CT when the spectroscopic states are on G2 or C2. There is only a ∼5% difference in population of these intrastrand CT states whether the GC tetrad is embedded in the $(GC)_5$ sequence or AT tract. There is also no significant population of the interstrand CT states. As shown in Table 2 (as well as Tables S1 and S4 in the SI), the averaged diabatic energies of the intrastrand CT states are approximately isoenergetic with the lowest bright states (and very similar whether in $(GC)_5$ or an AT tract), while the interstrand CT states lie approximately 0.6 eV higher in energy.

While the bases above and below the tetrad only have a small influence on the dynamics, the effect of the step is more noticeable. As shown in Figure 7, for CG steps the population transfer to the intrastrand CT states is less substantial than for GC, albeit they are always the most populated states following photoexcitation, involving ∼40% of the photoexcited population. Similar to GC, there is also no significant difference whether embedded in $(GC)_5$ or AT. As shown in Table 2, the intrastrand CT states are ∼0.3 eV less stable in the CG step than in GC, and with smaller couplings to the lowest bright states, in particular, for the bright states on C, explaining the lower population of the intrastrand CT states for initial excitation on this base for the CG steps. The effect of the step

Table 2. Averaged Diabatic Energies E_{ii} of the Lowest Bright States on Each Base and the Intra- and Interstrand CT States, as Well as the Absolute Value of the Couplings E_{ij} of the Bright States with the Corresponding Intrastrand CT State[a]

energy	GC in $(GC)_5$	GC in AT	CG in $(GC)_5$	CG in AT
G1(L_a)	5.310	5.318	5.313	5.311
G2(L_a)	5.316	5.319	5.315	5.306
C1($\pi\pi^*1$)	5.308	5.304	5.324	5.319
C2($\pi\pi^*1$)	5.318	5.312	5.316	5.321
G1 → C1-CT	5.277	5.226	5.582	5.547
G2 → C2-CT	5.292	5.246	5.577	5.561
G1 → C2(CT)	5.893	5.834	5.984	5.926
G2 → C1(CT)	5.911	5.905	5.900	5.906
coupling				
G1(L_a):G1 → C1-CT	0.090	0.069	0.048	0.069
C1($\pi\pi^*1$):G1 → C1-CT	0.087	0.077	0.024	0.019
G2(L_a):G2 → C2-CT	0.061	0.062	0.057	0.039
C2($\pi\pi^*1$): G2 → C2-CT	0.067	0.078	0.035	0.014

[a]From molecular dynamics snapshots of GC and CG steps in $(GC)_5$ or AT. In eV, parameterized by M05-2X/6-31G(d)/PCM(water) calculations.

correlates well with the analysis of the molecular dynamics simulations in the previous section, with the GC steps shown to be closer together and with more overlap of the bases than the CG steps, resulting in lower intrastrand CT energies, and stronger couplings to the bright states.

Turning to an analysis of the individual QD simulations, rather than averaged over the MD sampled structures, in Figure 8 we show the population of the intrastrand CT state, following excitation on the lowest bright state of each base in the same strand. The structures are GC tetrads extracted from the $(GC)_5$ MD simulation (with the corresponding plot for the

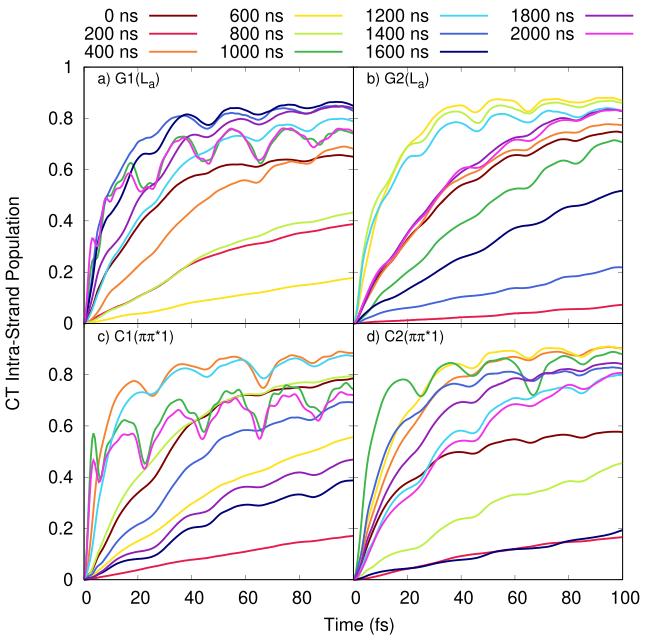

Figure 8. Population of the corresponding intrastrand CT state following initial excitation of (a) G1(L_a), (b) G2(L_a), (c) C1($\pi\pi^*1$), and (d) C2($\pi\pi^*2$) for each of the GC tetrad snapshots from the $(GC)_5$ MD simulation.

https://doi.org/10.1021/acs.jpcb.2c05688
J. Phys. Chem. B XXXX, XXX, XXX−XXX

CG tetrads shown in the SI, Figure S32). A number of things are immediately apparent from this figure. First, there is a large dispersion of the population of the CT state, ranging from virtually no population after 100 fs, to very quick and almost complete (>0.8) population. In fact, the average result shown in Figure 6 is somewhere in between these extremes. A second thing to notice is the asymmetry of the different strands. For example, the 600 ns structure has little population of the G1 → C1 CT state, while there is significant population of the G2 → C2 CT state, for excitations on strand 1 or 2, respectively. Third, there is also asymmetry between the bases on each strand. For example, the 800 ns structure has limited population of the CT state following excitation of G1(L_a), but much more significant population following excitation of C1($\pi\pi^*1$), while on strand 2 the opposite is true. As shown in Table S3 in the SI, these features are nicely correlated with the coupling of the bright state to the CT state. In the cases where there is limited population of the CT state, the population typically remains on the bright state of initial excitation, rather than transfer to any other state (see Figures collected in Section S4 of the SI for the complete dynamics of each snapshot). A final thing that can be observed in this figure are oscillations in the CT populations of certain snapshots. These are due to coherences with bright states on the same strand, as evidenced by the full population figures collected in Section S4 of the SI. Furthermore, for an example snapshot at 2000 ns that shows significant oscillations, we compute and plot the off diagonal elements of the density matrix $\rho_{LE,CT}(t) = \mathrm{Tr}\{|CT\rangle\langle LE|\hat{\rho}(t)\}$ for a more direct measure of the coherence, as shown in Figure S19. We noticed similar behavior for the population of a CT state in a GC Watson−Crick pair in ref 84. These coherences are essentially washed-out when the populations are averaged over a number of simulations.

CONCLUDING REMARKS

In this work we have defined a suitable computational strategy for the inclusion of thermal fluctuations in the study of the excited state behavior of DNA fragments, tackling (i) the computation of the steady state absorption and ECD spectra and (ii) the simulation of the population transfer between bright and CT states, on the ultrafast time-scale. Our approach, following a recipe commonly used in the study of MCAs,[85−87] exploits MD simulations to generate a certain number of structures to be used in subsequent QM-based analysis. It is clear that such a strategy can be adopted if the "QM-based" part is sufficiently accurate to provide reliable indications and, at the same time, its computational cost is low enough to be applied to a sufficiently large number of structures.

Without aiming to provide fully statistically representative results, this test study shows that these requirements are met by our FrDEx and FrD-LVC methods. Both methods are rooted in a fragment diabatization procedure, which, based on a reference TD-DFT calculation, provides the electronic parameters for study the photoactivated dynamics of a MCA (energy, coupling) in terms of diabatic states localized on each chromophore.[29,31] This is a "natural" approach for excitonic models, which describe MCAs on the basis of their constituent chromophores.[85,88,89] Moreover, it is also suitable for QD studies,[90,91] especially when coupled with MD. Of course, the choice of the diabatic basis is not unique[92] and one could imagine a scenario in which delocalized states are used instead of monomer-based states. However, in a fluctuating system, where transient localization can always occur (e.g., due to strand opening motions), the monomer basis is likely the most suitable interpretive framework.

In this study, we tried to define the best strategy to use FrDEx within B-DNA. Based on our experience on GQ,[29,30] we used dimers (including only the closest bases) for H_{inter} terms and assessed two models (trimer strand and tetrad, see Scheme 2) for the computation of H_{intra}. The rolling trimer strand approach appears the most suitable one, providing similar accuracy to the tetrad approach, with a smaller computational cost. Moreover, in principle we could also obtain CT couplings (at least those with the stacked bases) directly from the rolling trimer calculation, further reducing the number of dimer calculations necessary to compute H_{inter} terms.

Thanks to the diabatization procedure, FrDEx can include the effect the surrounding monomers on the local excitations and consider CT states, the most suitable approach for a closely stacked MCA such as DNA. The importance of these effects in DNA are clearly shown by the computed absorption and the ECD spectra of $(GC)_5$. In both cases FrDEx spectra are very close to the reference TD-M05-2X ones, the most significant discrepancy being a slight blue-shift of the maximum of the positive lobe at ∼290 nm. More importantly, they reproduce fairly well the shape of the experimental ECD spectrum of $(GC)_9$, though the overall spectrum is significantly blue-shifted with respect to the experimental one, mirroring the inaccuracies of the reference TD-M05-2X calculations. The important hypochromic effect associated with the formation of DNA duplex is also fully captured. A standard excitonic Hamiltonian, including only isolated local excitations and no CT states, fails to reproduce the hypochromic effect and the computed ECD spectrum is in worse quantitative agreement with the reference ones, being further blue-shifted with respect to the FrDEx one and underestimating the intensity of the positive peak in the red-wing. On the other hand, the computed ECD spectra are still in fairly good qualitative agreement with the experiments, and the computational cost of FHC calculations is smaller than the FrDEx ones, making it more suitable to be applied to a more extensive sampling of the MD simulations. However, it cannot be taken for granted what the effect of the FHC approximations with other DNA sequences are. In perspective, in future studies, it could be interesting to integrate FrDEx and FHC, using the former one to test the accuracy of FHC on a restricted number of snapshots. By using a larger, more statistically relevant, number of structures, it could be possible to get additional insights on the structural effects ruling the shape of the ECD spectra, increasing the possibility of using the analysis of the ECD spectra to monitor the DNA structural dynamics.

For what concerns QD simulations, we show here that, thanks to the huge advance in propagation methods such as MCTDH, FrD-LVC can describe the ultrafast dynamics of a system with four nucleobases, including a large number of excited states and vibrational modes. Here, to show the potentialities of our method, we analyzed two different steps (CG and GC, with four bases) in two difference sequences ($(CG)_5$ and ACGT/AGCT), simulating 100 fs of the dynamics on 11 different structures. On this ground, it could be rather straightforward to sample more structures, especially if focusing on a single step within a well-defined sequence, or, even more easily, in a single DNA strand. Actually, the main

https://doi.org/10.1021/acs.jpcb.2c05688
J. Phys. Chem. B XXXX, XXX, XXX−XXX

limitation of our simulations are those related to the use of LVC model (see ref 31 for a more detailed discussion), which makes it possible to study only the ultrafast part of the excited state dynamics, due to the reliance on a harmonic description of the vibrational modes, Moreover, we do not consider the out-of-plane motion, and therefore, we cannot properly describe the "monomer"-like deactivation routes, which involve severe distortion of the nucleobases planarity.[15] However, these deactivation routes are characterized by time constants >200 fs,[77,78] that is, slower than the time regime studied here. In the ≤100 fs time regime we study, we have highlighted that for some structures that have suboptimal stacking, CT states are not significantly populated, and the population remains on the locally excited states, opening up the possibility of monomer deactivation at later times. Finally, we work within the static disorder limit, that is, considering intermolecular arrangements too slow to move during the 100 fs photodynamics. In this limit, the coupling with MD simulations is a very promising approach, because it allows sampling of the slower vibrational degrees of freedom, for which the use of harmonic approximation is less reliable.[93,94] Also in this case, in perspective, FrD-LVC could be profitably used to complement surface-hopping semiclassical simulations methods[95−97] to assess the importance of nuclear quantum effects and identify the diabatic states ruling the photoactivated dynamics.

Besides these methodological aspects, our simulations confirm that UV excitation of oligoGC leads to the effective and fast population of intrastrand CT states,[48,54,72] which, according to previous studies, can then be involved in PT reactions.[47,48,54] We here show that this transfer is more effective for GC than for CG steps, since the former are more closely stacked than the latter. Moreover, this conclusion is valid when GC/CG steps are included both in an oligoGC or in an oligoAT sequence, paving the route for future studies, experimental or computational, that explicitly tackle the dependence of the photoactivated dynamics of a given fragment on the DNA sequence to which it is inserted.

■ ASSOCIATED CONTENT

Supporting Information

The Supporting Information is available free of charge at https://pubs.acs.org/doi/10.1021/acs.jpcb.2c05688.

Additional methodological details, additional analysis of the MD results of the FrD-LVC simulations, and additional FrDEx spectra (PDF)

■ AUTHOR INFORMATION

Corresponding Author

Roberto Improta − *Consiglio Nazionale delle Ricerche, Istituto di Biostrutture e Bioimmagini (IBB-CNR), I-80145 Napoli, Italy; DTU Chemistry, Technical University of Denmark, DK-2800 Kongens Lyngby, Denmark;* orcid.org/0000-0003-1004-195X; Email: robimp@unina.it, roberto.improta@cnr.it

Authors

Haritha Asha − *Consiglio Nazionale delle Ricerche, Istituto di Biostrutture e Bioimmagini (IBB-CNR), I-80145 Napoli, Italy*

James A. Green − *Consiglio Nazionale delle Ricerche, Istituto di Biostrutture e Bioimmagini (IBB-CNR), I-80145 Napoli, Italy; Institute of Physical and Theoretical Chemistry, Goethe University Frankfurt, 60438 Frankfurt am Main, Germany;* orcid.org/0000-0002-5036-3104

Luciana Esposito − *Consiglio Nazionale delle Ricerche, Istituto di Biostrutture e Bioimmagini (IBB-CNR), I-80145 Napoli, Italy*

Lara Martinez-Fernandez − *Departamento de Química, Facultad de Ciencias and Institute for Advanced Research in Chemistry (IADCHEM), Universidad Autònoma de Madrid, 28049 Madrid, Spain;* orcid.org/0000-0001-5361-9390

Fabrizio Santoro − *Consiglio Nazionale delle Ricerche, Istituto di Chimica dei Composti Organo Metallici (ICCOM-CNR), SS di Pisa, Area della Ricerca, I-56124 Pisa, Italy;* orcid.org/0000-0003-4402-2685

Complete contact information is available at: https://pubs.acs.org/10.1021/acs.jpcb.2c05688

Notes

The authors declare no competing financial interest.

■ ACKNOWLEDGMENTS

R.I. thanks the Otto Mønsted Foundation for supporting his stay at DTU and CNR (progetti@cnr/UCATG4 and Nutrage) for financial support. F.S. thanks progetti@cnr/UCATG4 and the Bilateral Programme CNR-Royal Society 2021−2022 for financial support.

■ DEDICATION

This paper is dedicated to Vincenzo Barone on the occasion of his 70th birthday, for our long and fruitful collaboration on the study of the photoactivated dynamics of DNA and of its components, after starting with one of us the journey on this topic in 2004, focusing on the lowest energy excited states of uracil in water.

■ REFERENCES

(1) Ma, H.; Wan, C.; Wu, A.; Zewail, A. H. DNA folding and melting observed in real time redefine the energy landscape. *Proc. Natl. Acad. Sci. U. S. A.* **2007**, *104*, 712−716.

(2) Rodger, A. In *Encyclopedia of Biophysics*; Roberts, G. C. K., Ed.; Springer: Berlin, Heidelberg, 2013; pp 2714−2718.

(3) Nwokeoji, A. O.; Kilby, P. M.; Portwood, D. E.; Dickman, M. J. Accurate Quantification of Nucleic Acids Using Hypochromicity Measurements in Conjunction with UV Spectrophotometry. *Anal. Chem.* **2017**, *89*, 13567−13574.

(4) Kypr, J.; Kejnovskà, I.; Renčiuk, D.; Vorlíčkovà, M. Circular dichroism and conformational polymorphism of DNA. *Nucleic Acids Res.* **2009**, *37*, 1713−1725.

(5) Vorlickova, M.; Kejnovskà, I.; Bednářovà, K.; Renčiuk, D.; Kypr, J. Circular Dichroism Spectroscopy of DNA: From Duplexes to Quadruplexes. *Chirality* **2012**, *24*, 691.

(6) Tinoco, I. Hypochromism in Polynucleotides. *J. Am. Chem. Soc.* **1960**, *82*, 4785.

(7) Felsenfeld, G.; Hirschman, S. Z. A neighbor-interaction analysis of the hypochromism and spectra of DNA. *J. Mol. Biol.* **1965**, *13*, 407.

(8) Improta, R.; Douki, T.*DNA Photodamage: From Light Absorption to Cellular Responses and Skin Cancer*; Royal Society of Chemistry, 2021.

(9) Martínez Fernández, L.; Santoro, F.; Improta, R. Nucleic Acids as a Playground for the Computational Study of the Photophysics and Photochemistry of Multichromophore Assemblies. *Acc. Chem. Res.* **2022**, *55*, 2077−2087.

(10) Gustavsson, T.; Markovitsi, D. Fundamentals of the Intrinsic DNA Fluorescence. *Acc. Chem. Res.* **2021**, *54*, 1226−1235.

(11) Schreier, W. J.; Gilch, P.; Zinth, W. Early Events of DNA Photodamage. *Annu. Rev. Phys. Chem.* **2015**, *66*, 497−519.
(12) Chen, J.; Zhang, Y.; Kohler, B. Excited states in DNA strands investigated by ultrafast laser spectroscopy. *Top. Curr. Chem.* **2014**, *356*, 39.
(13) Crespo-Hernández, C. E.; Cohen, B.; Hare, P. M.; Kohler, B. Ultrafast Excited-State Dynamics in Nucleic Acids. *Chem. Rev.* **2004**, *104*, 1977−2020.
(14) Barbatti, M.; Borin, C. A.; Ullrich, S.*Photoinduced Phenomena in Nucleic Acids I: Nucleobases in the Gas Phase and in Solvents*; Springer International Publishing: Cham, Switzerland, 2015; Vol. *355*, pp 1−358.
(15) Improta, R.; Santoro, F.; Blancafort, L. Quantum mechanical studies on the photophysics and the photochemistry of nucleic acids and nucleobases. *Chem. Rev.* **2016**, *116*, 3540−3593.
(16) Šponer, J.; Bussi, G.; Krepl, M.; Banáš, P.; Bottaro, S.; Cunha, R. A.; Gil-Ley, A.; Pinamonti, G.; Poblete, S.; Jurečka, P.; Walter, N. G.; Otyepka, M. RNA Structural Dynamics As Captured by Molecular Simulations: A Comprehensive Overview. *Chem. Rev.* **2018**, *118*, 4177−4338.
(17) Marko, A.; Denysenkov, V.; Margraf, D.; Cekan, P.; Schiemann, O.; Sigurdsson, S. T.; Prisner, T. F. Conformational Flexibility of DNA. *J. Am. Chem. Soc.* **2011**, *133*, 13375−13379.
(18) Cheatham, T. E., III; Kollman, P. A. Molecular Dynamics Simulation of Nucleic Acids. *Annu. Rev. Phys. Chem.* **2000**, *51*, 435−471.
(19) Voityuk, A. A.; Siriwong, K.; Rösch, N. Charge transfer in DNA. Sensitivity of electronic couplings to conformational changes. *Phys. Chem. Chem. Phys.* **2001**, *3*, 5421−5425.
(20) Voityuk, A. A. Electronic couplings and on-site energies for hole transfer in DNA: Systematic quantum mechanical/molecular dynamic study. *J. Chem. Phys.* **2008**, *128*, 115101.
(21) Voityuk, A. A. Conformational dependence of the electronic coupling for singlet excitation energy transfer in DNA. An INDO/S study. *Phys. Chem. Chem. Phys.* **2010**, *12*, 7403−7408.
(22) Voityuk, A. A. Effects of dynamic disorder on exciton delocalization and photoinduced charge separation in DNA. *Photochem. Photobiol. Sci.* **2013**, *12*, 1303−1309.
(23) Martinez-Fernandez, L.; Improta, R. In *Photodamage: From Light Absorption to Cellular Responses and Skin Cancer*; Improta, R., Douki, T., Eds.; The Royal Society of Chemistry, 2022; pp 17−36.
(24) Cadet, J.; Grand, A.; Douki, T. In *Photoinduced Phenomena in Nucleic Acids II: DNA Fragments and Phenomenological Aspects*; Barbatti, M., Borin, A. C., Ullrich, S., Eds.; Springer International Publishing: Cham, 2015; pp 249−275.
(25) Schreier, W. J.; Schrader, T. E.; Koller, F. O.; Gilch, P.; Crespo-Hernández, C. E.; Swaminathan, V. N.; Carell, T.; Zinth, W.; Kohler, B. Thymine Dimerization in DNA Is an Ultrafast Photoreaction. *Science* **2007**, *315*, 625−629.
(26) Conti, I.; Martínez-Fernández, L.; Esposito, L.; Hofinger, S.; Nenov, A.; Garavelli, M.; Improta, R. Multiple Electronic and Structural Factors Control Cyclobutane Pyrimidine Dimer and 6−4 Thymine−Thymine Photodimerization in a DNA Duplex. *Chemistry − A European Journal* **2017**, *23*, 15177−15188.
(27) Banyasz, A.; Douki, T.; Improta, R.; Gustavsson, T.; Onidas, D.; Vayá, I.; Perron, M.; Markovitsi, D. Electronic Excited States Responsible for Dimer Formation upon UV Absorption Directly by Thymine Strands: Joint Experimental and Theoretical Study. *J. Am. Chem. Soc.* **2012**, *134*, 14834−14845.
(28) Improta, R. Photophysics and Photochemistry of Thymine Deoxy-Dinucleotide in Water: A PCM/TD-DFT Quantum Mechanical Study. *J. Phys. Chem. B* **2012**, *116*, 14261−14274.
(29) Green, J. A.; Asha, H.; Santoro, F.; Improta, R. Excitonic Model for Strongly Coupled Multichromophoric Systems: The Electronic Circular Dichroism Spectra of Guanine Quadruplexes as Test Cases. *J. Chem. Theory Comput.* **2021**, *17*, 405−415.
(30) Asha, H.; Green, J. A.; Martinez-Fernandez, L.; Esposito, L.; Improta, R. Electronic Circular Dichroism Spectra of DNA Quadruple Helices Studied by Molecular Dynamics Simulations and Excitonic Calculations including Charge Transfer States. *Molecules* **2021**, *26*, 4789.
(31) Green, J. A.; Yaghoubi Jouybari, M.; Asha, H.; Santoro, F.; Improta, R. Fragment Diabatization Linear Vibronic Coupling Model for Quantum Dynamics of Multichromophoric Systems: Population of the Charge-Transfer State in the Photoexcited Guanine−Cytosine Pair. *J. Chem. Theory Comput.* **2021**, *17*, 4660−4674.
(32) Jouybari, M. Y.; Green, J. A.; Improta, R.; Santoro, F. The Ultrafast Quantum Dynamics of Photoexcited Adenine−Thymine Basepair Investigated with a Fragment-based Diabatization and a Linear Vibronic Coupling Model. *J. Phys. Chem. A* **2021**, *125*, 8912−8924.
(33) Padula, D.; Jurinovich, S.; Di Bari, L.; Mennucci, B. Simulation of Electronic Circular Dichroism of Nucleic Acids: From the Structure to the Spectrum. *Chemistry − A European Journal* **2016**, *22*, 17011−17019.
(34) Di Meo, F.; Pedersen, M. N.; Rubio-Magnieto, J.; Surin, M.; Linares, M.; Norman, P. DNA Electronic Circular Dichroism on the Inter-Base Pair Scale: An Experimental−Theoretical Case Study of the AT Homo-Oligonucleotide. *J. Phys. Chem. Lett.* **2015**, *6*, 355−359.
(35) Loco, D.; Jurinovich, S.; Bari, L. D.; Mennucci, B. A fast but accurate excitonic simulation of the electronic circular dichroism of nucleic acids: how can it be achieved? *Phys. Chem. Chem. Phys.* **2016**, *18*, 866−877.
(36) Makkonen, E.; Rinke, P.; Lopez-Acevedo, O.; Chen, X. Optical Properties of Silver-Mediated DNA from Molecular Dynamics and Time Dependent Density Functional Theory. *International Journal of Molecular Sciences* **2018**, *19*, 2346.
(37) Gattuso, H.; Assfeld, X.; Monari, A. Modeling DNA Electronic Circular Dichroism by QM/MM Methods and Frenkel Hamiltonian. *Theor. Chem. Acc.* **2015**, *134*, 36.
(38) Norman, P.; Parello, J.; Polavarapu, P. L.; Linares, M. Predicting near-UV electronic circular dichroism in nucleosomal DNA by means of DFT response theory. *Phys. Chem. Chem. Phys.* **2015**, *17*, 21866−21879.
(39) Sobolewski, A. L.; Domcke, W.; Hättig, C. Tautomeric selectivity of the excited-state lifetime of guanine/cytosine base pairs: The role of electron-driven proton-transfer processes. *Proc. Natl. Acad. Sci. U.S.A* **2005**, *102*, 17903−17906.
(40) Schwalb, N. K.; Temps, F. Ultrafast Electronic Relaxation in Guanosine is Promoted by Hydrogen Bonding with Cytidine. *J. Am. Chem. Soc.* **2007**, *129*, 9272.
(41) Schwalb, N. K.; Michalak, T.; Temps, F. Ultrashort Fluorescence Lifetimes of Hydrogen-Bonded Base Pairs of Guanosine and Cytidine in Solution. *J. Phys. Chem. B* **2009**, *113*, 16365.
(42) Markwick, P. R. L.; Doltsinis, N. L.; Schlitter, J. Probing irradiation induced DNA damage mechanisms using excited state Car-Parrinello molecular dynamics. *J. Chem. Phys.* **2007**, *126*, 045104.
(43) Röttger, K.; Marroux, H. J. B.; Grubb, M. P.; Coulter, P. M.; Bohnke, H.; Henderson, A. S.; Galan, M. C.; Temps, F.; Orr-Ewing, A. J.; Roberts, G. M. Ultraviolet Absorption Induces Hydrogen-Atom Transfer in G·C Watson-Crick DNA Base Pairs in Solution. *Angew. Chem., Int. Ed.* **2015**, *54*, 14719.
(44) Biemann, L.; Kovalenko, S. A.; Kleinermanns, K.; Mahrwald, R.; Markert, M.; Improta, R. Excited State Proton Transfer is Not Involved in the Ultrafast Deactivation of Guanine-Cytosine Pair in Solution. *J. Am. Chem. Soc.* **2011**, *133*, 19664.
(45) Martínez-Fernández, L.; Banyasz, A.; Markovitsi, D.; Improta, R. Topology Controls the Electronic Absorption and Delocalization of Electron Holes in Guanine Quadruplexes. *Chem.—Eur. J.* **2018**, *24*, 15185−15189.
(46) Groenhof, G.; Schäfer, L. V.; Boggio-Pasqua, M.; Goette, M.; Grubmüller, H.; Robb, M. A. Ultrafast Deactivation of an Excited Cytosine-Guanine Base Pair in DNA. *J. Am. Chem. Soc.* **2007**, *129*, 6812−6819.
(47) Martinez-Fernandez, L.; Improta, R. Photoactivated proton coupled electron transfer in DNA: insights from quantum mechanical calculations. *Faraday Discuss.* **2018**, *207*, 199−216.

https://doi.org/10.1021/acs.jpcb.2c05688
J. Phys. Chem. B XXXX, XXX, XXX−XXX

(48) Zhang, Y.; de La Harpe, K.; Beckstead, A. A.; Improta, R.; Kohler, B. UV-induced proton transfer between DNA strands. *J. Am. Chem. Soc.* **2015**, *137*, 7059−7062.
(49) Zhang, Y.; de La Harpe, K.; Beckstead, A. A.; Martínez-Fernández, L.; Improta, R.; Kohler, B. Excited-state dynamics of DNA duplexes with different H-bonding motifs. *J. Phys. Chem. Lett.* **2016**, *7*, 950−954.
(50) Bucher, D. B.; Schlueter, A.; Carell, T.; Zinth, W. Watson−Crick Base Pairing Controls Excited-State Decay in Natural DNA. *Angew. Chem., Int. Ed.* **2014**, *53*, 11366−11369.
(51) Zuluaga, C.; Spata, V. A.; Matsika, S. Benchmarking Quantum Mechanical Methods for the Description of Charge-Transfer States in π-Stacked Nucleobases. *J. Chem. Theory Comput.* **2021**, *17*, 376−387.
(52) Spata, V. A.; Matsika, S. Role of Excitonic Coupling and Charge-Transfer States in the Absorption and CD Spectra of Adenine-Based Oligonucleotides Investigated through QM/MM Simulations. *J. Phys. Chem. A* **2014**, *118*, 12021−12030.
(53) Nogueira, J. J.; Plasser, F.; González, L. Electronic delocalization, charge transfer and hypochromism in the UV absorption spectrum of polyadenine unravelled by multiscale computations and quantitative wavefunction analysis. *Chem. Sci.* **2017**, *8*, 5682.
(54) Zhang, Y.; de La Harpe, K.; Kohl, F. R.; Kohler, B. Isotopic substitution affects excited state branching in a DNA duplex in aqueous solution. *Chem. Commun.* **2019**, *55*, 4174−4177.
(55) Mills, J. B.; Hagerman, P. J. Origin of the intrinsic rigidity of DNA. *Nucleic Acids Res.* **2004**, *32*, 4055−4059.
(56) Hunter, C. A. Sequence-dependent DNA Structure: The Role of Base Stacking Interactions. *J. Mol. Biol.* **1993**, *230*, 1025−1054.
(57) Gotoh, O.; Tagashira, Y. Stabilities of nearest-neighbor doublets in double-helical DNA determined by fitting calculated melting profiles to observed profiles. *Biopolymers* **1981**, *20*, 1033−1042.
(58) Köppel, H.; Domcke, W.; Cederbaum, L. S. Multimode Molecular Dynamics Beyond the Born-Oppenheimer Approximation. *Adv. Chem. Phys.* **1984**, *57*, 59.
(59) Li, S.; Olson, W. K.; Lu, X.-J. Web 3DNA 2.0 for the analysis, visualization, and modeling of 3D nucleic acid structures. *Nucleic Acids Res.* **2019**, *47*, W26−W34.
(60) Berendsen, H. J. C.; Grigera, J. R.; Straatsma, T. P. The missing term in effective pair potentials. *J. Phys. Chem.* **1987**, *91*, 6269−6271.
(61) Joung, I. S.; Cheatham, T. E., III Determination of Alkali and Halide Monovalent Ion Parameters for Use in Explicitly Solvated Biomolecular Simulations. *J. Phys. Chem. B* **2008**, *112*, 9020−9041.
(62) Zgarbová, M.; Šponer, J.; Otyepka, M.; Cheatham, T. E., III; Galindo-Murillo, R.; Jurečka, P. Refinement of the Sugar-Phosphate Backbone Torsion Beta for AMBER Force Fields Improves the Description of Z- and B-DNA. *J. Chem. Theory Comput.* **2015**, *11*, 5723−5736.
(63) Berendsen, H. J. C.; Postma, J. P. M.; van Gunsteren, W. F.; DiNola, A.; Haak, J. R. Molecular dynamics with coupling to an external bath. *J. Chem. Phys.* **1984**, *81*, 3684−3690.
(64) Case, D. A.; Cheatham, T. E., III; Darden, T.; Gohlke, H.; Luo, R.; Merz, K. M., Jr.; Onufriev, A.; Simmerling, C.; Wang, B.; Woods, R. J. The Amber biomolecular simulation programs. *J. Comput. Chem.* **2005**, *26*, 1668−1688.
(65) Lu, X.; Olson, W. K. 3DNA: a software package for the analysis, rebuilding and visualization of three?dimensional nucleic acid structures. *Nucleic Acids Res.* **2003**, *31*, 5108−5121.
(66) Lu, X.-J.; Bussemaker, H. J.; Olson, W. K. DSSR: an integrated software tool for dissecting the spatial structure of RNA. *Nucleic Acids Res.* **2015**, *43*, e142−e142.
(67) Frisch, M. J.; Trucks, G. W.; Schlegel, H. B.; Scuseria, G. E.; Robb, M. A.; Cheeseman, J. R.; Scalmani, G.; Barone, V.; Petersson, G. A.; et al.*Gaussian 16*, Revision C.01; Gaussian Inc.: Wallingford, CT, 2016.
(68) Zhao, Y.; Truhlar, D. G. Density Functionals with Broad Applicability in Chemistry. *Acc. Chem. Res.* **2008**, *41*, 157−167.
(69) Tomasi, J.; Mennucci, B.; Cammi, R. Quantum Mechanical Continuum Solvation Models. *Chem. Rev.* **2005**, *105*, 2999−3094.
(70) Iozzi, M. F.; Mennucci, B.; Tomasi, J.; Cammi, R. Excitation energy transfer (EET) between molecules in condensed matter: A novel application of the polarizable continuum model (PCM). *J. Chem. Phys.* **2004**, *120*, 7029−7040.
(71) Santoro, F.; Green, A. J.Overdia1.0, a Fortran 90 code for the parametrization of model Hamiltonians based on a maximum-overlap diabatisation, available free of charge at http://www.iccom.cnr.it/overdia-en/.
(72) Martinez Fernandez, L.; Green, J. A.; Yaghoubi Jouybari, M.; Esposito, L.; Santoro, F.; Improta, R.*to be submitted*. 2022,.
(73) Dreuw, A.; Head-Gordon, M. Single-Reference ab Initio Methods for the Calculation of Excited States of Large Molecules. *Chem. Rev.* **2005**, *105*, 4009.
(74) Isborn, C. M.; Mar, B. D.; Curchod, B. F. E.; Tavernelli, I.; Martínez, T. J. The Charge Transfer Problem in Density Functional Theory Calculations of Aqueously Solvated Molecules. *J. Phys. Chem. B* **2013**, *117*, 12189.
(75) Kozma, B.; Tajti, A.; Demoulin, B.; Izsák, R.; Nooijen, M.; Szalay, P. G. A New Benchmark Set for Excitation Energy of Charge Transfer States: Systematic Investigation of Coupled Cluster Type Methods. *J. Chem. Theory Comput.* **2020**, *16*, 4213.
(76) Avila Ferrer, F. J.; Cerezo, J.; Stendardo, E.; Improta, R.; Santoro, F. Insights for an Accurate Comparison of Computational Data to Experimental Absorption and Emission Spectra: Beyond the Vertical Transition Approximation. *J. Chem. Theory Comput.* **2013**, *9*, 2072−2082.
(77) Martínez-Fernández, L.; Pepino, A. J.; Segarra-Martí, J.; Jovaišait, J.; Vaya, I.; Nenov, A.; Markovitsi, D.; Gustavsson, T.; Banyasz, A.; Garavelli, M.; Improta, R. Photophysics of Deoxycytidine and 5-Methyldeoxycytidine in Solution: A Comprehensive Picture by Quantum Mechanical Calculations and Femtosecond Fluorescence Spectroscopy. *J. Am. Chem. Soc.* **2017**, *139*, 7780−7791.
(78) Karunakaran, V.; Kleinermanns, K.; Improta, R.; Kovalenko, S. A. Photoinduced Dynamics of Guanosine Monophosphate in Water from Broad-Band Transient Absorption Spectroscopy and Quantum-Chemical Calculations. *J. Am. Chem. Soc.* **2009**, *131*, 5839−5850.
(79) Jurinovich, S.; Cupellini, L.; Guido, C. A.; Mennucci, B. EXAT: EXcitonic analysis tool. *J. Comput. Chem.* **2018**, *39*, 279−286.
(80) Wang, H.; Thoss, M. Multilayer formulation of the multi-configuration time-dependent Hartree theory. *J. Chem. Phys.* **2003**, *119*, 1289−1299.
(81) Wang, H. Multilayer Multiconfiguration Time-Dependent Hartree Theory. *J. Phys. Chem. A* **2015**, *119*, 7951−7965.
(82) Worth, G. A.; Giri, K.; Richings, G. W.; Beck, M. H.; Jäckle, A.; Meyer, H.-D.*QUANTICS Package*, Version 1.1; University of Birmingham: Birmingham, U.K., 2015.
(83) Worth, G. Quantics: A general purpose package for Quantum molecular dynamics simulations. *Comput. Phys. Commun.* **2020**, *248*, 107040.
(84) Green, J. A.; Gómez, S.; Worth, G.; Santoro, F.; Improta, R. Solvent Effects on Ultrafast Charge Transfer Population: Insights from the Quantum Dynamics of Guanine-Cytosine in Chloroform. *Chemistry − A European Journal* **2022**, *28*, No. e202201731.
(85) Segatta, F.; Cupellini, L.; Garavelli, M.; Mennucci, B. Quantum Chemical Modeling of the Photoinduced Activity of Multichromophoric Biosystems. *Chem. Rev.* **2019**, *119*, 9361−9380.
(86) Cupellini, L.; Calvani, D.; Jacquemin, D.; Mennucci, B. Charge transfer from the carotenoid can quench chlorophyll excitation in antenna complexes of plants. *Nature Comm* **2020**, *11*, 662.
(87) Curutchet, C.; Mennucci, B. Quantum Chemical Studies of Light Harvesting. *Chem. Rev.* **2017**, *117*, 294−343.
(88) Hestand, N. J.; Spano, F. C. Expanded Theory of H- and J-Molecular Aggregates: The Effects of Vibronic Coupling and Intermolecular Charge Transfer. *Chem. Rev.* **2018**, *118*, 7069−7163.
(89) Brixner, T.; Hildner, R.; Köhler, J.; Lambert, C.; Würthner, F. Exciton Transport in Molecular Aggregates − From Natural Antennas

https://doi.org/10.1021/acs.jpcb.2c05688
J. Phys. Chem. B XXXX, XXX, XXX−XXX

to Synthetic Chromophore Systems. *Adv. Energy Mater.* **2017**, *7*, 1700236.
(90) Popp, W.; Brey, D.; Binder, R.; Burghardt, I. Quantum Dynamics of Exciton Transport and Dissociation in Multichromophoric Systems. *Annu. Rev. Phys. Chem.* **2021**, *72*, 591−616.
(91) Schröter, M.; Ivanov, S.; Schulze, J.; Polyutov, S.; Yan, Y.; Pullerits, T.; Kühn, O. Exciton−vibrational coupling in the dynamics and spectroscopy of Frenkel excitons in molecular aggregates. *Phys. Rep.* **2015**, *567*, 1−78.
(92) Shu, Y.; Varga, Z.; Kanchanakungwankul, S.; Zhang, L.; Truhlar, D. G. Diabatic States of Molecules. *J. Phys. Chem. A* **2022**, *126*, 992−1018.
(93) Cerezo, J.; Aranda, D.; Avila Ferrer, F. J.; Prampolini, G.; Santoro, F. Adiabatic-Molecular Dynamics Generalized Vertical Hessian Approach: A Mixed Quantum Classical Method To Compute Electronic Spectra of Flexible Molecules in the Condensed Phase. *J. Chem. Theory Comput.* **2020**, *16*, 1215−1231.
(94) Segalina, A.; Aranda, D.; Green, J. A.; Cristino, V.; Caramori, S.; Prampolini, G.; Pastore, M.; Santoro, F. How the Interplay among Conformational Disorder, Solvation, Local, and Charge-Transfer Excitations Affects the Absorption Spectrum and Photoinduced Dynamics of Perylene Diimide Dimers: A Molecular Dynamics/Quantum Vibronic Approach. *J. Chem. Theory Comput.* **2022**, *18*, 3718−3736.
(95) Zobel, J. P.; Heindl, M.; Plasser, F.; Mai, S.; González, L. Surface Hopping Dynamics on Vibronic Coupling Models. *Acc. Chem. Res.* **2021**, *54*, 3760−3771.
(96) Spencer, J.; Gajdos, F.; Blumberger, J. FOB-SH: Fragment orbital-based surface hopping for charge carrier transport in organic and biological molecules and materials. *J. Chem. Phys.* **2016**, *145*, 064102.
(97) Peng, W.-T.; Brey, D.; Giannini, S.; Dell'Angelo, D.; Burghardt, I.; Blumberger, J. Exciton Dissociation in a Model Organic Interface: Excitonic State-Based Surface Hopping versus Multiconfigurational Time-Dependent Hartree. *J. Phys. Chem. Lett.* **2022**, *13*, 7105−7112.

https://doi.org/10.1021/acs.jpcb.2c05688
J. Phys. Chem. B XXXX, XXX, XXX−XXX